5-20-1985

Gulf Stream Meanders: Observations on the Deep Currents

W. E. Johns

D. Randolph Watts

JOURNAL OF GEOPHYSICAL RESEARCH, VOL. 90, NO. C3, PAGES 4819–4832, MAY 20, 1985

Gulf Stream Meanders: Observations on the Deep Currents

W. E. JOHNS AND D. R. WATTS

Graduate School of Oceanography, University of Rhode Island, Kingston

During 1979–1980, an array of inverted echo sounders (IES) and three deep current meter moorings were deployed on the continental slope 100–200 km northeast of Cape Hatteras, North Carolina. This array continuously monitored the path of the Gulf Stream and the deep currents under it. The mean currents at two sites 1000 m off the bottom near the northern edge of the stream were veered to the right of the mean surface path, indicating a deep inflow to the stream. Mean currents 500 and 1000 m off the bottom 50 km farther offshore were northeastward, nearly colinear with the surface Gulf Stream path. The deep velocity fluctuations are characterized by a transition from transverse flow aligned with the local bathymetry for periods longer than about 12 days to fluctuations with a cross-stream orientation for shorter periods. For periods between 4 days and 1 month, cross-stream movements of the Gulf Stream temperature front are vertically coherent and nearly barotropic, based on correlations between the IES-measured stream path and deep temperature fluctuations. Temperature fluctuations at the current meter sites lead cross-stream (positive onshore) velocity fluctuations by approximately 90°. Consideration of the nondiffusive fluctuating heat equation for deep layers suggests a three-term balance between local rate of change, cross-stream horizontal advection, and vertical advection of temperature, with the first two being of like sign. Kinematically, this requires $|wT_z| > |vT_y|$, so that parcel trajectories in the cross-stream plane are inclined at angles steeper than the mean cross-stream slope of the isotherms. Eddy energy conversion between the fluctuations and the mean field in deep layers is predominantly baroclinic, with *e*-folding growth time scales of approximately 10 days.

1. INTRODUCTION

The vertical coherence, structure, and energetics of fluctuations in the Gulf Stream have been topics of great interest for many years. Several intensive studies have been carried out in the Florida Current [*Brooks and Niiler*, 1977; *Duing*, 1975; *Duing et al.*, 1977] and in the Gulf Stream along the continental shelf south of Cape Hatteras [*Brooks and Bane*, 1983; *Bane et al.*, 1981; *Lee and Atkinson*, 1983]. These studies have generally shown high vertical coherence of velocity and temperature fluctuations on 1–2 week time scales. The available evidence suggests that these fluctuations are caused by vertically coherent, barotropic meanders of the lateral velocity and density structure of the Gulf Stream. Associated with these meanders are upwelling regions and "spin-off" or "frontal" eddies [*Lee*, 1975], which propagate downstream with the meanders at speeds of between 35 and 50 km/d [*Brooks and Bane*, 1981].

Similar current observations spanning the water column are not available for deep water regions northeast of Cape Hatteras, owing primarily to difficulties in placing tall moorings within the intense Gulf Stream flow. Of the deep current observations existing in this region [*Luyten*, 1977; *Schmitz et al.*, 1970], direct comparisons with Gulf Stream path variability were possible only during a 5-week time period when thermal path data obtained by ship or aircraft were available. Interpretation of these data suggested that cross-stream motions associated with time scales of approximately 5 days are vertically coherent [*Robinson et al.*, 1974] but that fluctuations at lower frequencies may not be [*Schmitz et al.*, 1970]. *Luyten* [1977] moored an extensive array of deep current meters under the Gulf Stream near 70°W and found large eddy variability, characterized by bursts of bottom-intensified meridional flow of short zonal scale (≤ 50 km) but longer meridional scale (~ 150 km). Subsequently, *Hogg* [1981] and *Thompson* [1977] showed that these measurements were consistent with the kinematics and disperion of topographic Rossby waves. The relationship, if any, between the deep currents in this region and the variability of the surface Gulf Stream path has not been established.

During 1979–1980, we collected a 12-month record from an array of seven inverted echo sounders (IES) and four deep current meters deployed 100 to 200 km northeast of Cape Hatteras in 2000–4000 m water depth. This array continuously monitored the path of the Gulf Stream and the deep currents under it. In an earlier paper [*Watts and Johns*, 1982] we described in detail the measurement techniques using IES's in the Gulf Stream, and we presented an observational dispersion relationship for meanders in this region. In this paper we concentrate on the deep currents, their energetics, and their relationship to the Gulf Stream path variability measured by IES.

2. OBSERVATIONS

Current meter moorings were set at three locations in 3000–4000 m water depth during 1979 and 1980. The sites were chosen to be within the historical envelope of meandering of the Gulf Stream, in a region where meanders are known to exhibit rapid spatial growth yet where the lateral excursions are still small enough so that a limited array would adequately span and monitor variations within the stream. The sites are shown in Figure 1. Currents and temperatures 1000 m off the bottom were obtained at site 1 during May–November 1979 (CM791), at site 2 during May–August 1979 (CM792) and November 1979 to July 1980 (CM802), and at site 3 during November 1979–July 1980 (CM803). On the latter deployment (November 1979 to July 1980), site 2 had a second current meter at 500 m off the bottom (CM802L) that was a Niskin winged current meter. All others were vector-averaging current meters. The spacing between current meter sites was approximately 50 km; sites 1 and 2 were zonally oriented within the Gulf Stream, and sites 2 and 3 were separated across stream. During these deployments, IES sites were maintained

Paper number 5C0051.
0148-0227/85/005C-0051$05.00

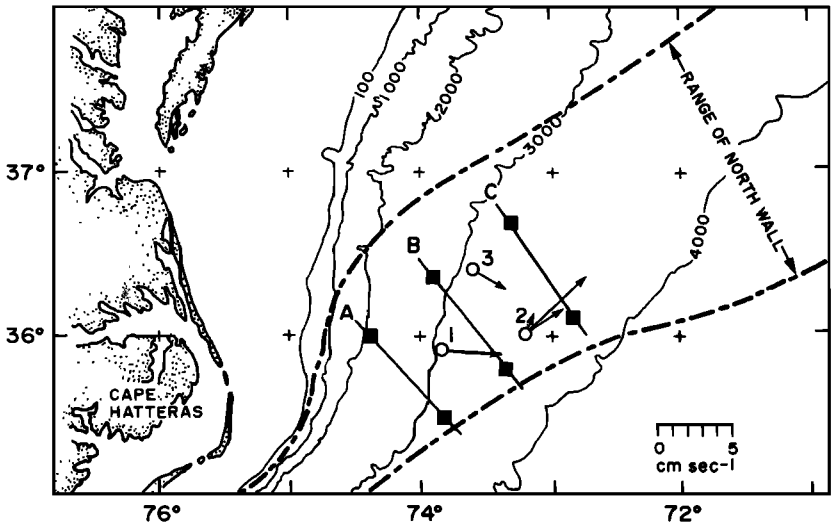

Fig. 1. Survey area. IES sites are shown as black squares, forming three sections: A, upstream; B, central; and C, downstream. Current meter sites are shown as open circles, with vectors indicating mean currents. At site 2 the shortest vector is the 9-month mean of 500 m off the bottom (site 2L), and the intermediate and longest vectors are means of 1000 m off the bottom for the 3-month and 9-month deployments, respectively. The north-wall envelope (long and short dashes) has been constructed from historical paths determined from shipboard (XBT and towed thermistor) and AXBT surveys.

at the locations shown in Figure 1 to monitor fluctuations in the location of the Gulf Stream's north wall (15°C at 200 m) according to the method described in *Watts and Johns* [1982; hereafter WJ82].

The velocity and temperature time series at each of the sites are shown in Figure 2 and labeled according to the above codes. All of the data records have been low-pass filtered with a 24-hour half-width Gaussian window and then subsampled at 12-hour intervals.

3. Results

The velocity and temperature time series (Figure 2) exhibit variability on time scales ranging from a few days to about 1 month. The visual coherence between sites is generally quite poor, except for a few events that can be traced (e.g., between sites 1 and 2 during late May and June and between sites 2 and 3 during mid-June). During these periods, current reversals at the western, upslope sites (1 and 3) appear to lead those at the eastern, downslope site (2) by 1–2 days. Surprisingly, strong extended periods of southward flow at site 3 (near the northern edge of the Gulf Stream) often coincide with strong northward or northeastward flows at site 2 (farther offshore within the stream). The currents at 500 and 1000 m off the bottom on mooring 2 are very coherent, with consistently lower speeds at the deeper meter, except for occasional events of bottom-intensified flow (into the northeast quadrant around January 3 and April 8 and into the southwest quadrant around March 1). These events coincide with rapid temperature changes of typically 0.1–0.2°C.

The means and variances of the deep current and temperature records are summarized in Table 1 together with the current meter depths and bottom depths at each of the sites. The variance in the v component (north) is typically larger than that of the u component (east). The mean currents (the vectors in Figure 1) at sites 1 and 3 in 3000 m water depth are veered roughly 45° to the right of the mean surface path, whereas at site 2 in 3700 m water depth the mean current is approximately colinear with the surface mean path. This veering to the right of the surface current may be associated with an inflow from the slope water, or it may be a manifestation of the vertical veering of current associated with advection of heat [*Bryden*, 1975]. For the observed weekly-to-monthly time scales of motion (shown below) one may assume that measurements separated by 1 month are statistically independent, and therefore a rough estimate of the number of degrees of freedom (M) associated with each estimate of the mean current can be obtained by dividing the respective record length by 1 month. The standard deviation of the mean is then estimated by dividing the sample standard deviation of each velocity component by the square root of M. Mean current standard deviations estimated in this manner are indicated in parentheses in Table 1. These error estimates imply that the inflow component at site 3 is significantly nonzero, whereas at site 1 it is marginally nonzero.

The kinetic, potential, and total eddy energy spectra for each site are shown in Figure 3. All spectra and cross spectra computed here were formed by breaking up the records into 48-day segments, removing the mean, windowing with a Hanning (cosine) window in the time domain, Fourier transforming, and ensemble averaging. Segments were overlapped by 24 days (i.e., 50%). The resulting adjacent spectral estimates at 48 days, 24 days, 16 days, etc., have effective bandwidths of 0.0312 cpd and are thus overlapped in the frequency domain by 33% (i.e., adjacent estimates are 67% independent). Some of the cross spectra (shown later) have subsequently been averaged over two frequency bands to improve the reliability of estimates.

The eddy energy is defined by

$$E = \frac{1}{2}\rho_0\left\{\overline{u'^2} + \overline{v'^2} + \frac{g\alpha}{|\bar{\theta}_z|}\cdot\overline{T'^2}\right\}$$

provided that the vertical potential temperature gradient $\bar{\theta}_z$ is known and that the T/S relation is sufficiently well defined that $\rho'/\rho_0 = \alpha(\bar{T}, \bar{S})T'$ is a reasonable approximation of the fluctuating density [*Bryden*, 1979]. The first two terms in brackets above represent the eddy kinetic energy, and the last term is eddy potential energy. The ratio $\alpha/\bar{\theta}_z$ varies from site to site, ranging from approximately 11 to 15 cm/°C^2; $\bar{\theta}_z$ is

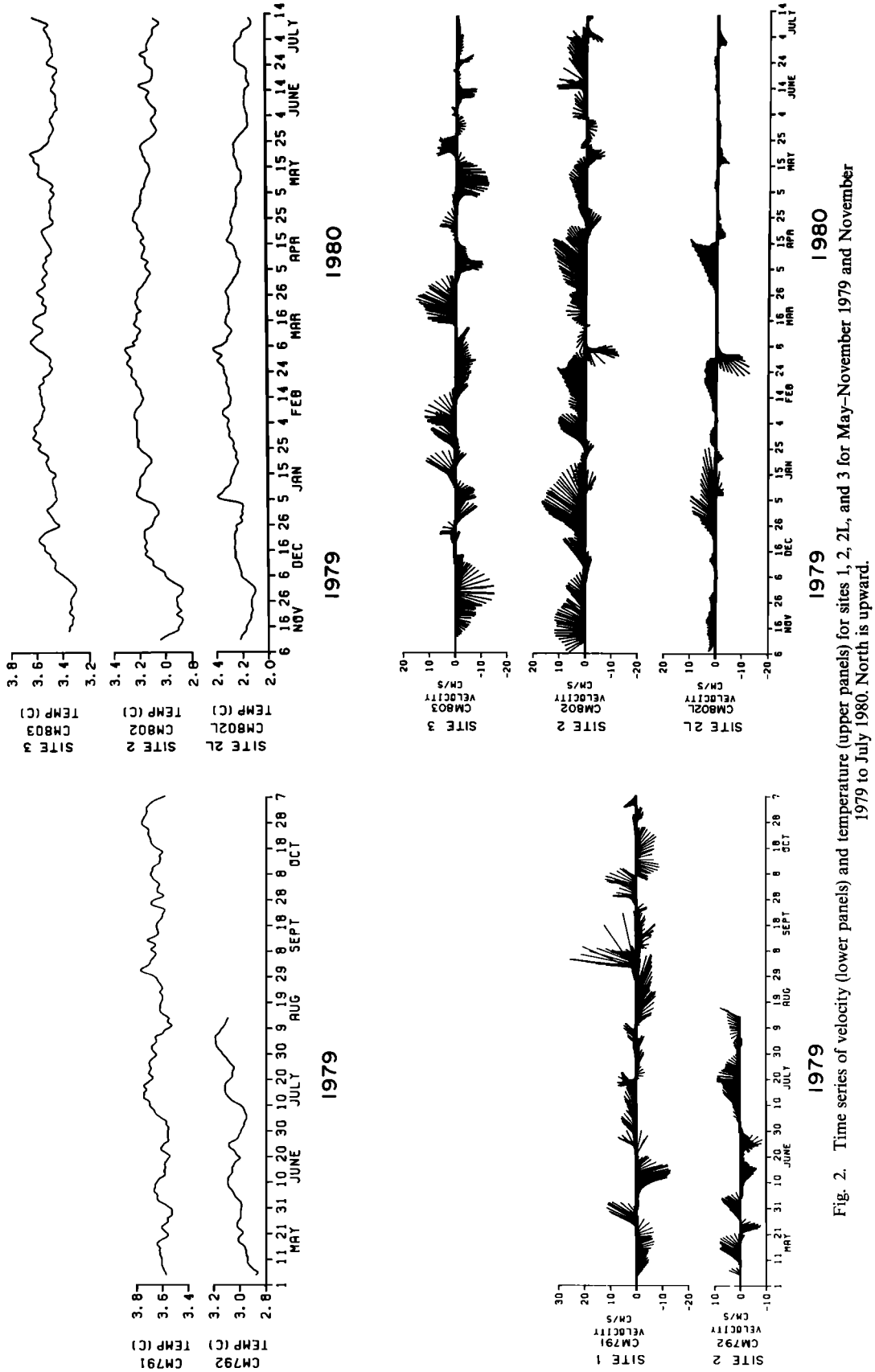

Fig. 2. Time series of velocity (lower panels) and temperature (upper panels) for sites 1, 2, 2L, and 3 for May–November 1979 and November 1979 to July 1980. North is upward.

TABLE 1. Mooring Statistics

Site	Current Meter Record	Latitude, °N	Longitude, °W	Duration, days	Bottom Depth, m	Current Meter Depth, m	T, °C Mean	T, °C σ	u, cm/s Mean	u, cm/s σ	v, cm/s Mean	v, cm/s σ
1	CM791	35°51.3′	73°50.2′	185	3070	1955	3.640	0.058	4.2 (±1.6)	3.8	−0.3 (±2.4)	5.8
2	CM792	35°55.7′	73°13.7′	101	3690	2685	3.038	0.073	2.5 (±1.5)	2.7	1.6 (±2.6)	4.7
2	CM802	35°55.8′	73°13.7′	241	3680	2665	3.127	0.094	4.1 (±1.5)	4.2	3.6 (±1.8)	5.1
2L	CM802L	35°55.8′	73°13.7′	241	3680	3170	2.194	0.066	0.6 (±1.2)	3.4	0.8 (±1.0)	2.8
3	CM803	36°18.0′	73°37.0′	241	3070	2060	3.489	0.073′	2.2 (±1.3)′	3.5′	−1.2 (±2.0)′	5.6

The parameter u is the east component of velocity, v is the north component of velocity. The number in parentheses after each mean velocity estimate is the standard deviation of the mean, assuming a monthly time scale (e.g., 6 degrees of freedom for a 6-month record); σ is the sample standard deviation of a quantity.

calculated from available hydrographic and "Pegasus" data (see section 4.1), and α is calculated from *Wright and Worthington*'s [1970] standard western North Atlantic deep water [θS] curve. Uncertainties in α (10%) and $\bar{\theta}_z$ (15%) introduce an additional ±25% error into the eddy potential energy estimates.

The eddy kinetic energy and eddy potential energy are similar in size, differing most at sites 1 and 2, where kinetic energy is 1.5 to 2 times larger than potential energy over a broad band from 24 to 4 days. Figure 4 compares eddy kinetic energy at all sites. At low frequencies the eddy kinetic energy at all sites 1000 m off the bottom is similar, but at site 2L (500 m off the bottom) it is smaller by about a factor of 2. For periods less than 10 days the eddy kinetic energy spectra for the three sites 1000 m off the bottom diverge, remaining largest at site 1. Site 1 is almost directly beneath the near-surface high-velocity axis of the Gulf Stream, while sites 2 and 3 are offshore and onshore of this central axis, respectively. At the current meter depths near 2000 m, all three moorings are within the cyclonic portion of the deep Gulf Stream.

The dynamical signatures of the deep current fluctuations are most clearly illustrated by computing rotary spectra [*Fofonoff*, 1969]; the variance ellipses so produced are shown in Figure 5. We have divided the variance into two bands—periods between 4 and 10 days and periods greater than 10 days—based on the marked change in orientation of the major axes that occurred at all sites near 10 days.

The 4–10 day variance ellipses are smaller by almost an order of magnitude than the long-period ellipses and tend to be more isotropic. Yet they are still somewhat elongated and point consistently NNW-SSE, approximately across the mean direction of flow (051°T) of the Gulf Stream during this period. The low-frequency ellipses are quite elongated, with major axes of approximately 30 cm^2/s^2. These motions reflect a strong bottom constraint, similar to topographic Rossby wave motions observed in water depths shallower than 4000 m during the 1974 Woods Hole Oceanographic Institution (WHOI) "Rise Array" [*Luyten*, 1977] and also near WHOI site "D" (39°10′N, 70°W) [*Thompson and Luyten*, 1976]. In section 5 we examine the properties of these motions and discuss consistency with topographic Rossby wave (TRW) properties in greater detail. The 4–10 day fluctuations can flow at large angles relative to the bathymetry, and their cross-stream orientation suggests a correlation with lateral translations of the Gulf Stream. This topic is explored in section 4.

In the sections that follow we shall adopt two coordinate rotations onto which the currents will be projected. Subscript "b" refers to a system aligned with the local bathymetry such that v_b points up the slope and u_b points along the slope. The orientations of the isobaths at sites 1, 2, and 3 are 001°, 025°, and 014°T, respectively, obtained by fitting a line segment of 40-km length (approximately one Rossby radius) along the isobaths at each mooring location. Subscript "s" refers to a system aligned with the mean near-surface Gulf Stream path determined by the IES array such that v_s points cross stream (321°T) and u_s points downstream (051°T). In all cases, z is positive upward.

4. GULF STREAM MEANDERS

4.1. *Vertical Coherence and Structure*

Displacements of the Gulf Stream axis at periods between 4 days and 1 month have been shown to be significantly coherent over the 100 km distance separating sections A and C, with phase lags indicating downstream propagation at speeds of 20–40 km/d (WJ82). The displacement spectra $G(Y)$ at sections A, B, and C are red (spectral slopes of f^{-2} to f^{-3}), with no significant features otherwise. Another, perhaps more revealing, way to look at the data is to consider the spectral distribution of the rate of cross-stream displacement of the Gulf Stream axis, $G(\partial Y/\partial t) = \omega^2 G(Y)$, shown in Figure 6 for section B. The displacement rate, or lateral velocity, of the Gulf Stream axis is broadly peaked in the 4–10 day band, indicating simply a larger amplitude-to-frequency ratio in this band. It is therefore reasonable to expect that deep velocity fluctuations associated with the meandering process will stand out above the noise more clearly in this band than at either lower or higher frequencies.

Figure 7 shows time series of cross-stream velocity (v_s) and temperature (T) at site 3 along with the time series of northwall displacement (Y) along IES section B relative to its mean position ($Y = 0$). Several events of onshore/offshore movement (increasing/decreasing Y) with periods of approximately 10 days and less are clearly correlated with changes in T and v_s. Visually, temperature increases during these events are nearly in phase with onshore movements of the Gulf Stream, while v_s fluctuations lag T and Y, so that onshore flows correspond to decreasing temperatures and vice versa.

As a kinematic interpretation, let the location of the cross-stream temperature front at any depth z be given by the Fourier sum

$$Y(x_s, z, t) = \sum_n Y_n(z) e^{i\phi_n(z)} e^{ik_n(x_s - c_n t)}$$

Near-surface results (WJ82) indicate that such a linear superposition is a valid representation of the variability. $Y_n(z)$ is the

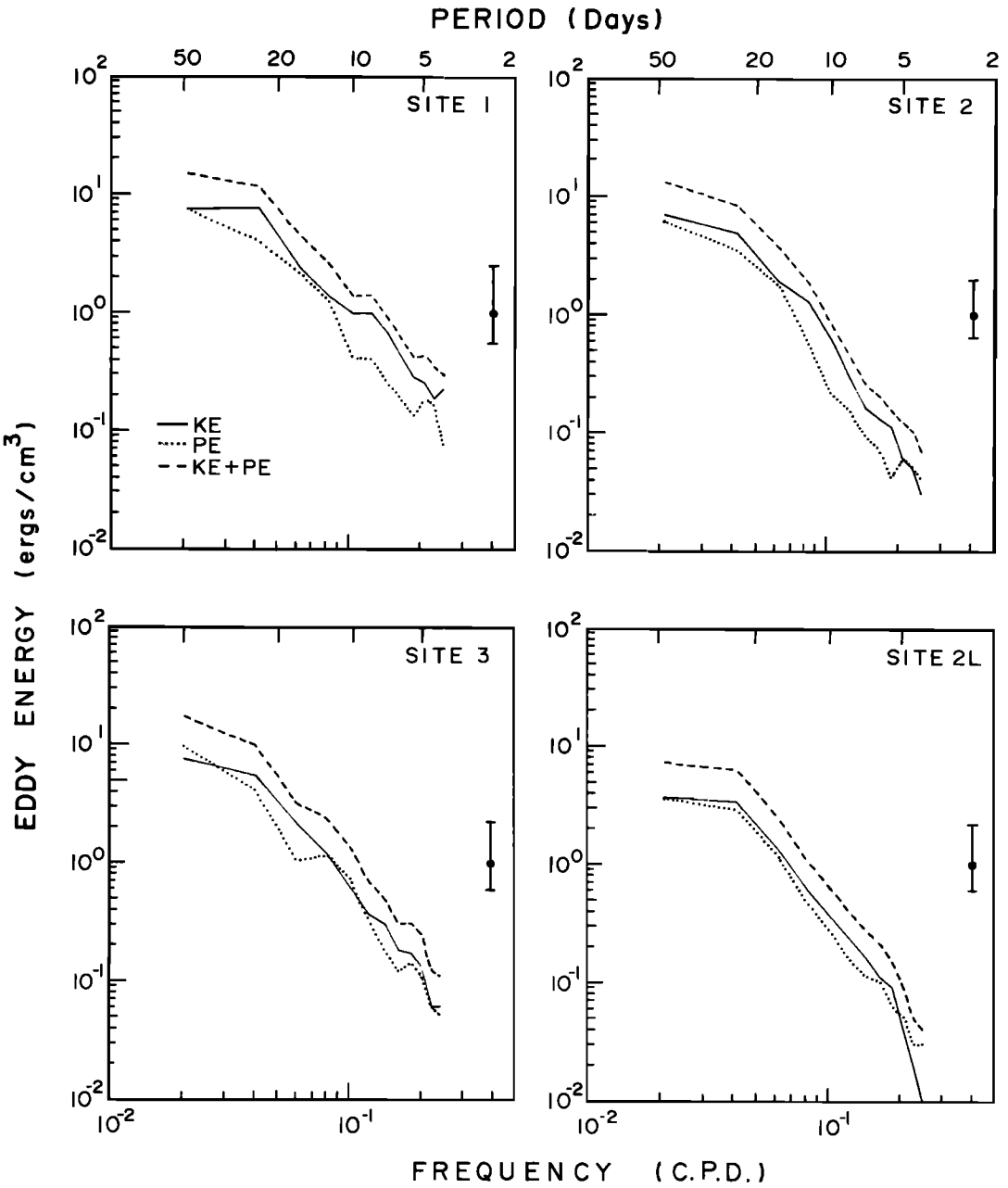

Fig. 3. Kinetic (KE), potential (PE), and total (KE + PE) eddy energy at current meter sites for periods from 4 to 48 days. Estimates at site 2 have approximately 18 degrees of freedom; sites 2L and 3, approximately 14 degrees of freedom each; and site 1, approximately 10 degrees of freedom.

depth-varying amplitude of a constituent wave n traveling in the mean downstream direction x_s at speed c_n. The phase ϕ_n of the wave may also vary with depth. (ϕ_n is related to, but distinct from, the vertical phase variation of the perturbation pressure found in baroclinic instability models [cf. *Eady*, 1949]. The temperature field is related hydrostatically to the vertical derivative of pressure.)

Historically, sections across the Gulf Stream have shown that the baroclinicity in the temperature (and density) field extends to the bottom. If temperature variations at a current meter, at some depth z_2, are produced entirely by lateral excursions of the deep temperature front, then

$$dY(z_2) = \frac{1}{[\bar{T}_{ys}(z_2)]} \cdot dT(z_2) \tag{1}$$

where $\bar{T}_{ys}$ is the mean cross-stream temperature gradient. A measure of how barotropic the lateral displacements are may be defined by the ratio of the deep front displacement $\hat{Y}_n(z_2)$ to the near-surface displacement $\hat{Y}_n(z_1)$ measured by IES, namely,

$$R_n = \frac{\hat{Y}_n(z_2)}{\hat{Y}_n(z_1)} = \frac{1}{\bar{T}_{ys}(z_2)} \cdot \left[\frac{G_{T_n}(z_2)}{G_{Y_n}(z_1)}\right]^{1/2} \tag{2}$$

In the above, G_{T_n} and G_{Y_n} are the temperature and displacement autospectra, respectively. The phase between $T(z_2)$ and $Y(z_1)$ is

$$\Phi_n = \phi_n(z_2) - \phi_n(z_1) \tag{3}$$

If T and Y are coherent, (2) gives an estimate of the ampli-

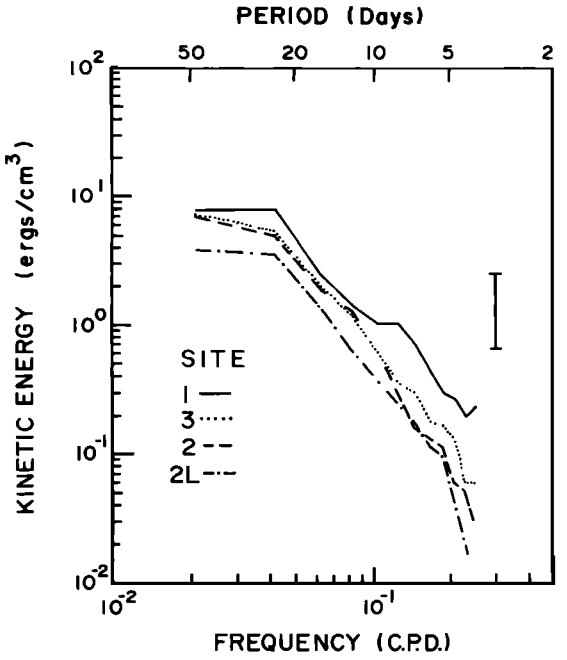

Fig. 4. Comparison of eddy kinetic energy at current meter sites 1, 2, and 3 (all 1000 m off the bottom) and 2L (500 m off the bottom).

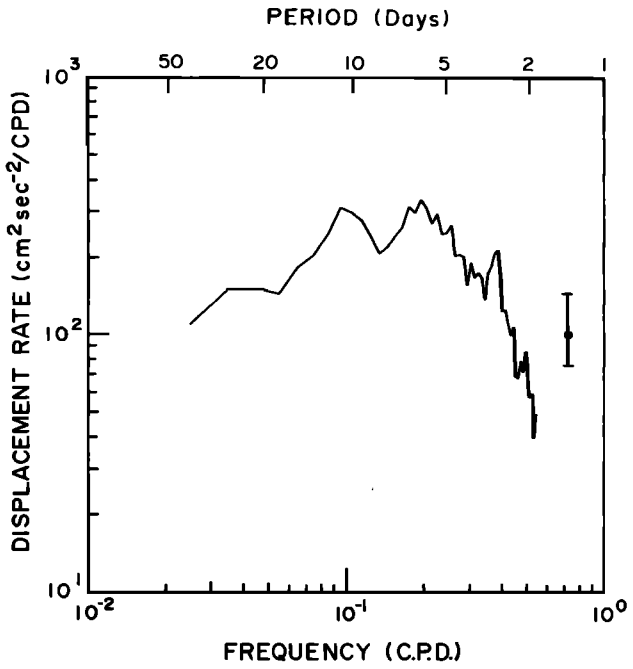

Fig. 6. One-year ensemble-averaged spectrum of the rate of path displacement (lateral velocity of the Gulf Stream axis) at IES section B (see Figure 1).

tude ratio R_n, and Φ_n gives an estimate of the vertical phase tilt. Operationally, the surface path displacement records $Y(x_s, z, t)$ are referenced to the appropriate along-stream position of the current meter sites by adjusting $\phi_n(z_1)$ to account for downstream propagation. This (small) phase shift is $k_n \delta x_s =$ $(2\pi f_n/c_n) \cdot \delta x_s$, where δx_s is the along-stream separation between sites, and where c_n is taken from the dispersion relation for Gulf Stream meanders reported in WJ82.

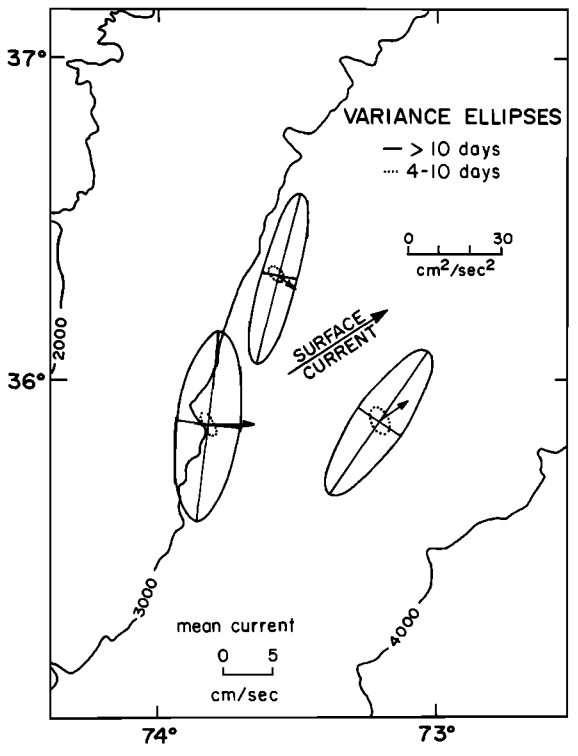

Fig. 5. Variance ellipses (according to upper scale) for sites 1000 m off the bottom. Large, solid ellipses indicate summed variance for periods greater than 10 days; small, dotted ellipses indicate summed variance for periods between 4 and 10 days. Vectors indicate mean current velocities (according to lower scale) 1000 m off the bottom.

In (2), $\bar{T}_{ys}(z_2)$ has been estimated from three hydrographic sections [*Barrett and Schmitz*, 1971; *Richardson and Knauss*, 1971; *Warren and Volkman*, 1968] and ten "Pegasus" sections (H. T. Rossby, unpublished data, 1984) across the Gulf Stream that were projected normal to the instantaneous path. From each section the average $\bar{T}_{ys}$ was computed over approximately one Rossby radius (40 km), centered on $T = 3.5°C$, $z = 2000$ m (appropriate to site 3); $T = 3.6°C$, $z = 2000$ m (site 1); and $T = 3.1°C$, $z = 2650$ m (site 2), yielding $\bar{T}_{ys} = 0.0045 \pm 0.0005°C/km$, $0.0045 \pm 0.0006°C/km$, and $0.0050 \pm 0.0007°C/km$, respectively. Since these are not significantly different, we use $\bar{T}_{ys} = 0.0050°C/km$ ($\pm 20\%$).

Figure 8 (*a*, *b*, *c*) shows the cross spectra between north-wall position Y along IES section B and temperatures at sites 1, 2, and 3. We have chosen to work exclusively with section B because it is central to the current meter array. Similar calculations, using sections A and C, yield essentially redundant results because of the high coherence and phase stability observed between north-wall displacements at sections A, B, and C.

The (Y, T) coherence at site 3, near the northern edge of the Gulf Stream, is quite high and significant at the 90% level for periods between 4 days and a month. At sites 1 and 2 the coherence is marginal, significant only at periods near 5 and 9 days at site 1 and at periods from 4 to 9 days and near 1 month at site 2. The low coherence (relative to significance levels) at site 1 may be due partly to the short $3\frac{1}{2}$-month record available there; however, the offshore decay in covariability at site 2 relative to that at site 3 is pronounced.

Figure 8*b* shows the vertical phase tilt $\phi_n(z_2) - \phi_n(z_1)$ with only significantly coherent points plotted. The phases are clustered near zero, ranging from $-35°$ to $+32°$. There is no apparent variation with frequency. Random phase errors at the 90% confidence level, based on the observed coherence

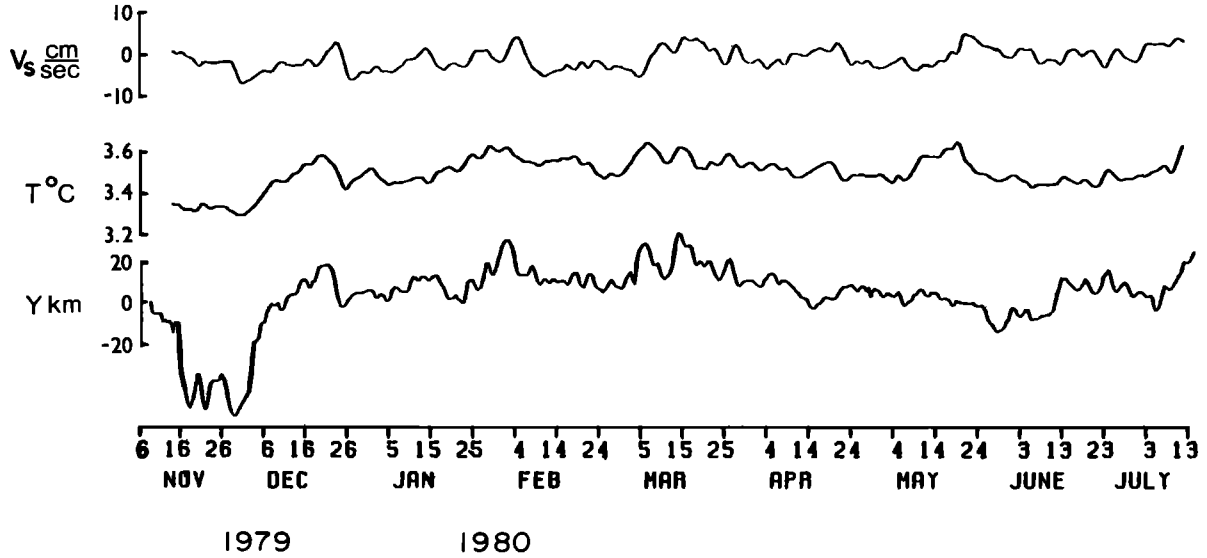

Fig. 7. Time series of path displacement (Y) along IES section B, with temperature (T) and cross-stream velocity (v_s) at current meter site 3 for the November 1979 to July 1980 deployment (see Figure 1 for section and site locations).

squared [*Bendat and Piersol*, 1971], are approximately $\pm 50°$ at site 2 ($\gamma^2 \sim 0.2$) and $\pm 30°$ at site 3 ($\gamma^2 \sim 0.5$), so the phase is insignificantly different from zero and significantly less than $\pm 90°$ for each estimate.

The amplitude ratio R_n is plotted in Figure 8*c* for significantly coherent points. R_n is close to 1.0 for periods near 1 month, with a small bias toward $R_n < 1.0$ near the 4–5 day periods. The average over all frequency bands is $R_n = 0.89 \pm 0.17$.

The front displacements are therefore essentially barotropic and in phase vertically. The vertical coherence is highest near the northern edge of the Gulf Stream at site 3, slightly shoreward of the mean position of the north wall. The sharp reduction in vertical coherence near 5-day periods at site 2 might be due to a relative increase in eddy noise there, or a real decrease in signal, or some combination of the two. However, the temperature variance in the 5–10 day band at site 2 is only about half that at site 3 (Figure 8*c*). Since the deep cross-stream temperature gradient is nearly equal at these two sites, this implies that the lateral displacement of deep isotherms in the 5–10 day band actually decreases as one moves offshore and/or deeper. This is not the case for periods near 1 month, which have similar coherence and R_n at both sites 2 and 3. At these long periods the meanders are barotropic and in phase, and they appear to span the full width of the mean baroclinic structure of the Gulf Stream.

4.2. *Kinematics: The Heat Balance and Vertical Motion*

By direct cross-spectral calculations, deep fluctuations in T and v_s can be seen to propagate downstream with characteristics similar to surface meanders (Figure 9). The average coherence squared of temperature fluctuations between sites 1 and 2 is approximately 0.5–0.6 in the 4-day to 1-month band, reaching a local minimum of ~ 0.3 near 9 days and dropping off sharply at periods shorter than 4 days. The downstream coherence squared of v_s, also shown in Figure 9, is significant between sites 1 and 2, with a frequency dependence similar to that of the temperature fluctuations. In the 5–10 day band the phase lag of v_s between these sites is remarkably consistent with WJ82's observed meander propagation curve sketched in

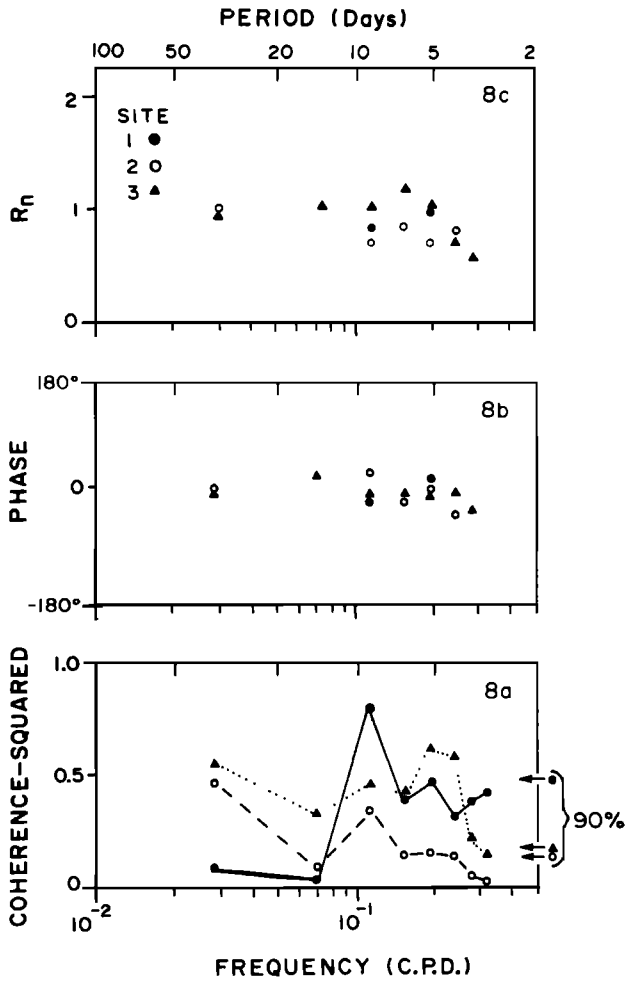

Fig. 8. (*a*) Coherence squared (γ^2), (*b*) phase (Φ_n; see equation (3)), and (*c*) amplitude ratio (R_n) cross spectra between Gulf Stream path displacements measured at IES section B (see Figure 1) and deep temperature fluctuations at current meter sites 1 (open circles), 2 (solid circles), and 3 (triangles). The 90% confidence levels for non-zero coherence squared are indicated by arrows at the right of Figure 8*a*. The approximate number of degrees of freedom are 9 for site 1, 36 for site 2, and 27 for site 3.

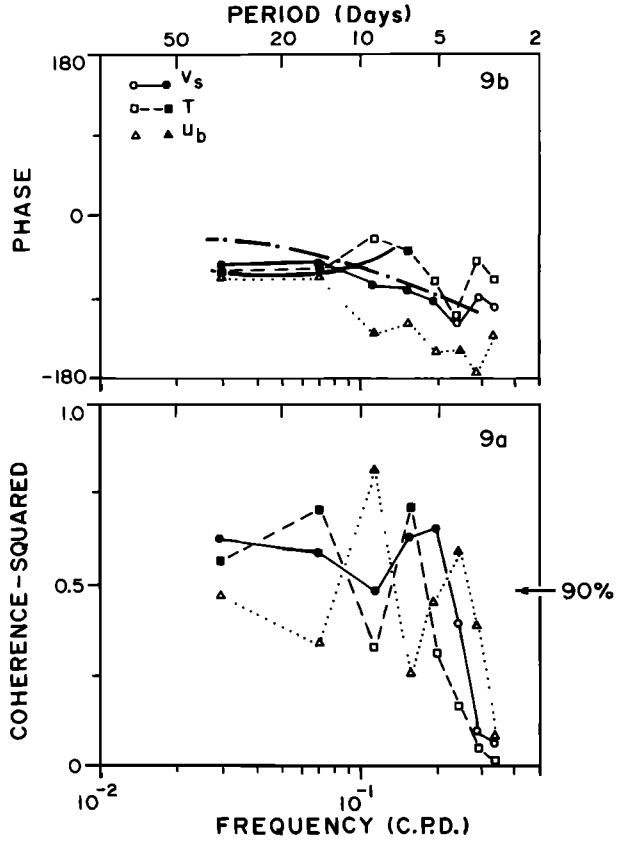

Fig. 9. (*a*) Coherence squared (γ^2) and (*b*) relative phase (ϕ) of the along-slope component of velocity (u_b, triangles), cross-stream velocity (v_s, circles), and temperature (T, squares) between 3½-month records at current meter sites 1 and 2. The closed symbols indicate points significantly coherent at the 90% confidence level. In the phase plot (*b*) the bold solid line indicates the expected phase difference based on observed topographic Rossby wave dispersion parameters; the bold dash-dot line shows the expected phase difference ϕ_n based on observed near-surface meander dispersion parameters. The 90% confidence level for nonzero coherence squared is shown at the right of Figure 9*a*.

Figure 9*b*. The temperature phase lags are more scattered but have the correct sign and similar trend. These observations suggest modeling the deep v_s and T variability as fluctuations that propagate downstream with the form $e^{ik(x_s - ct)}$.

Consider now the nondiffusive heat equation

$$\frac{\partial T}{\partial t} + u\frac{\partial T}{\partial x} + v\frac{\partial T}{\partial y} + w\frac{\partial \bar{\theta}}{\partial z} = 0$$

where $\partial\bar{\theta}/\partial z$ is the mean vertical potential temperature gradient. Let $T = \bar{T} + T'$, $u = \bar{u} + u'$, $v = \bar{v} + v'$, and $w = \bar{w} + w'$, where primes represent the variability of a quantity on an arbitrary time scale τ and where overbars represent the average of a quantity on time scales much larger than τ.

On time scales τ, and in stream coordinates ($\bar{T}_{xs} = 0$), the heat equation is

$$\frac{\partial T'}{\partial t} + \bar{u}_s\frac{\partial T'}{\partial x_s} + v_s'\frac{\partial \bar{T}}{\partial y_s} + \bar{v}_s\frac{\partial T'}{\partial y_s} + w'\frac{\partial \bar{\theta}}{\partial z} + \left[\frac{\partial}{\partial x_s}(u_s'T') + \frac{\partial}{\partial y_s}(v_s'T') + \frac{\partial}{\partial z}(w'\theta')\right] = -\left[\frac{\partial}{\partial x_s}\langle u_s T\rangle + \frac{\partial}{\partial y_s}\langle v_s T\rangle + \frac{\partial}{\partial z}\langle w\theta\rangle\right]$$

where angle brackets ($\langle\ \rangle$) denote an average over time scale τ, and the right-hand side therefore represents a possible contribution from the divergence of eddy heat flux caused by motions on time scales shorter than τ. For motions with periods from 4 days to 1 month the measurable leading terms $\partial T'/\partial t$ and $v'\partial\bar{T}/\partial y_s$ are of order 10^{-7}°C s^{-1}. Negligibly small terms, in the same units, are the divergence of eddy heat flux resulting from higher-frequency motions [$0(10^{-9})$] and $\bar{v}\partial T'/\partial y_s$ [$0(10^{-9})$], the latter estimated by differencing the rms temperature variability at sites 2 and 3. Based on typical velocity and temperature scales observed at the sites (u', $v' = 10$ cm/s; $T' = 0.1$°C) and assuming horizontal length scales L of 0(100 km), the ratio of the nonlinear terms to the leading linear advection term $v'\partial\bar{T}/\partial y_s$ is $T'/L\partial\bar{T}/\partial y_s \sim 20\%$. Therefore the nonlinear heat flux terms [$\partial(u'T')/\partial x$, $\partial(v'T')/\partial y$] may be significant but should not be as large as the linear terms. Direct results supporting this assertion are presented in *Johns* [1984], where the effects of nonlinear advection are explicitly taken into account in terms of the geostrophic veering method developed by *Bryden* [1975].

Consequently, the heat equation for 4-day to 1-month motions reduces approximately to the linear balance:

$$\frac{\partial T'}{\partial t} + \bar{u}_s\frac{\partial T'}{\partial x_s} + v_s'\frac{\partial \bar{T}}{\partial y_s} + w'\frac{\partial \bar{\theta}}{\partial z} = 0 \tag{4}$$

We now examine this fluctuating balance within the framework of temperature disturbances propagating as $T' \sim e^{ik(x_s - ct)}$, with c possibly complex, $c = c_r + ic_i$. Hence

$$-ikcT' + ik\bar{u}_sT' + v_s'\frac{\partial \bar{T}}{\partial y_s} + w'\frac{\partial \bar{\theta}}{\partial z} = 0 \tag{5}$$

Multiplying by T' and averaging,

$$ik(\bar{u}_s - c)\overline{T'^2} + \overline{T'v_s'}\frac{\partial \bar{T}}{\partial y_s} + \overline{T'w'}\frac{\partial \bar{\theta}}{\partial z} = 0$$

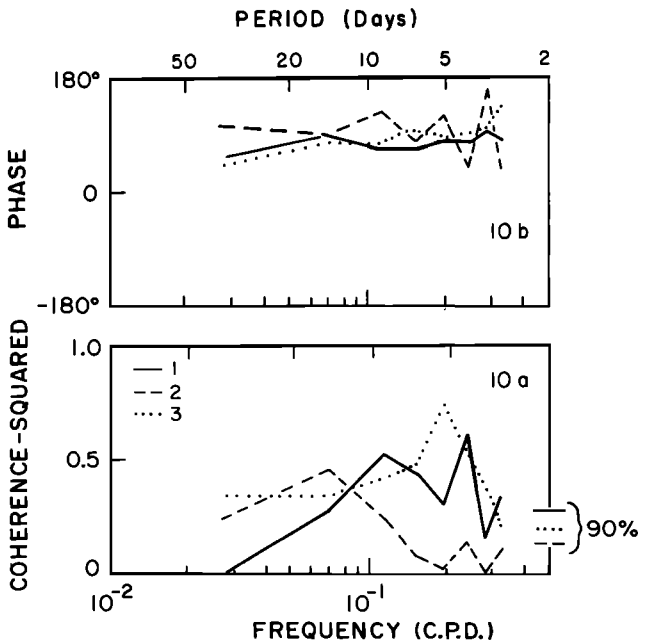

Fig. 10. (*a*) Coherence squared (γ^2) and (*b*) phase (ϕ) cross spectra between cross-stream velocity (v_s) and temperature (T) at sites 1 (solid line), 2 (dashed line), and 3 (dotted line). The 90% confidence levels for nonzero coherence squared for each site are indicated by a bracket at the right of Figure 10*a*.

TABLE 2. Correlation and Ratio Between Local Rate of Change of Temperature and Cross-Stream Advection of Temperature for Current Meter Sites 1000 m off the Bottom

Period Band, days	Correlation (T_t, vT_y)			Ratio (T_t/vT_y)		
	Site 1	Site 2	Site 3	Site 1	Site 2	Site 3
12–48	0.15 (0.47)	0.53 (0.35)	0.41 (0.40)	0.7	0.9	0.7
4–10	0.65 (0.34)	0.33 (0.25)	0.68 (0.29)	1.5	1.9	2.0

The 95% confidence levels for significantly nonzero correlation are indicated in parentheses beside each correlation coefficient estimate.

The real part of this equation,

$$kc_i\overline{T'^2} + \mathrm{Re}(\overline{T'v_s'})\frac{\partial\bar{T}}{\partial y_s} + \mathrm{Re}(\overline{T'w'})\frac{\partial\bar{\theta}}{\partial z} = 0 \qquad (6a)$$

governs the growth in time of the temperature fluctuations [*Bryden*, 1975] as a function of eddy heat fluxes [(T, $\vec{v}_s$) covariance] up or down the mean temperature gradients. The imaginary part,

$$k(\bar{u}_s - c_r)\overline{T'^2} + Im(\overline{T'v_s'})\frac{\partial\bar{T}}{\partial y_s} + Im(\overline{T'w'})\frac{\partial\bar{\theta}}{\partial z} = 0 \qquad (6b)$$

relates the oscillation in time of the temperature field to the quadrature spectra between temperature and velocity components.

The first two terms in (6*b*) can be estimated with knowledge of the mean fields $\bar{u}_s$ and $\bar{T}_{ys}$, dispersion properties (k, c_r), and measurements of the temperature autospectrum and (T, v_s) quadrature spectrum. Consequently, the last term, proportional to vertical advection, can be inferred within observational errors.

At the "steering level" ($\bar{u}_s = c_r$), (6*b*) implies that local temperature changes $\partial T'/\partial t$ are balanced by $\bar{u}_s\partial T'/\partial x_s$. Therefore, at this level, vertical and cross-stream advection must balance each other, in which case the flow in the y_s, z plane is inclined along isothermal surfaces; i.e., $w/v = (\partial z/\partial y)_\theta$. At deeper levels ($\bar{u}_s < c_r$), $\bar{u}_s\partial T'/\partial y_s$ plays a progressively decreasing role, and $\partial T'/\partial t$ is balanced by the sum of cross-stream and vertical advection. For the mean flows ($\bar{u}_s < 5$ cm/s) observed at these deep moorings, and for c_r in the range 20–40 cm/s (WJ82), (6*b*) becomes approximately

$$-\omega_r\overline{T'^2} - Im(\overline{T'v_s'})\left|\frac{\partial\bar{T}}{\partial y_s}\right| + Im(\overline{T'w'})\left|\frac{\partial\bar{\theta}}{\partial z}\right| = 0 \qquad (7)$$

after incorporating the signs of the mean temperature gradients and noting that $\omega_r = kc_r$. The key to this balance is the quadrature spectrum between T and v_s. Depending on its sign, cross-stream advection of temperature tends to either balance or reinforce local temperature change.

Figure 10 shows the cross spectrum between v_s and T at each of the current meter sites. The coherence squared at sites 2 and 3 exceeds the 90% confidence level for all periods longer than 10 days; however, the long-period estimate at site 1 shows very low coherence. An interesting feature of the v_s,T cross spectra is the different behavior in the 4–10 day band at sites 2 and 3. Near 5 days, the coherence at site 3 reaches a maximum, but at site 2 it is very small. This behavior is quite similar to that observed in the (Y, T) correlations.

At all sites, however, the phase is positive and close to 90°, with the exception of a few of the lowest-frequency estimates. The quadrature spectrum $Im(\overline{T'v_s'})$ is positive. Positive phase implies T leads v_s, consistent with the visual impression in Figure 7. Physically, onshore movements of the front (increasing T) are coupled with offshore velocities (negative v_s) and vice versa. Departures from this basic 90° phase relationship, of interest in determining the transfer of potential energy between the mean and fluctuating fields, are discussed in section 6.

With $Im(\overline{T'v_s'}) > 0$, the first two terms in (7) have the same sign, so local temperature changes are reinforced, on average, by cross-stream horizontal advection. Kinematically, this requires that vertical advection be of leading order in (4); i.e., $w/v > (\partial z/\partial y)_\theta$. Thus on average, deep parcel trajectories in the y_s, z plane are inclined at angles steeper than the mean cross-stream slope of the isotherms.

Table 2 lists the correlation coefficients between local rate of change of temperature and cross-stream advection of temperature within two bands, 4–10 days and 12–48 days, for each site. Also shown is the ratio of local rate of change to horizontal advection of temperature in these two bands. In all cases the correlations are positive. The correlation in the 4–10 day band is well above the 95% significance level. In the 12–48 day band the correlation is weaker (insignificant at site 1). For the 12–48 day motions, local rate of change of temperature and cross-stream advection of temperature estimated from (7) are of similar size, whereas in the 4–10 day band, local rate of change is 1.5 to 2 times larger than cross-stream advection. Particle trajectories of the motion are therefore inclined at a slope w/v, which is about 2 to 3 times the mean cross-stream slope of the isotherms $(\partial z/\partial y)_\theta$, depending on the frequency band. Deep isotherm slopes are approximately

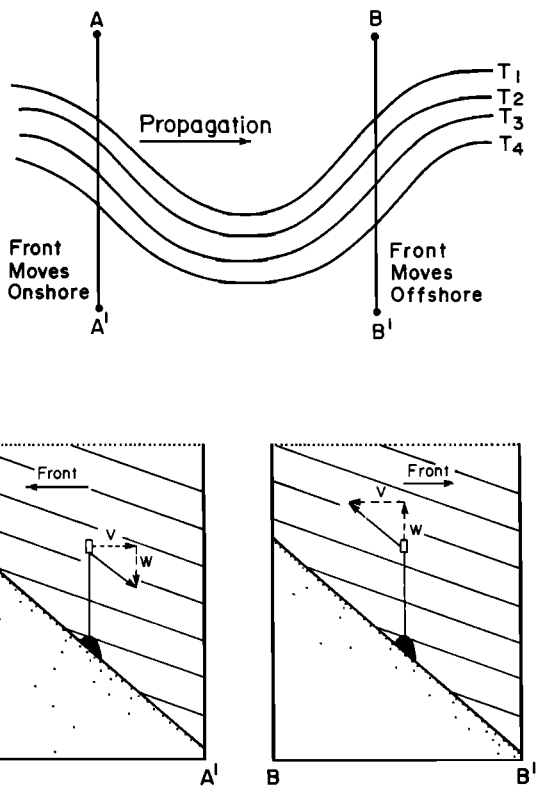

Fig. 11. Schematic illustration of propagating, wavelike deformation of deep temperature contours (top) and the relationship between cross-stream particle trajectories and lateral motion of the deep temperature front (bottom) along leading edges (AA') and trailing edges (BB') of a meander crest.

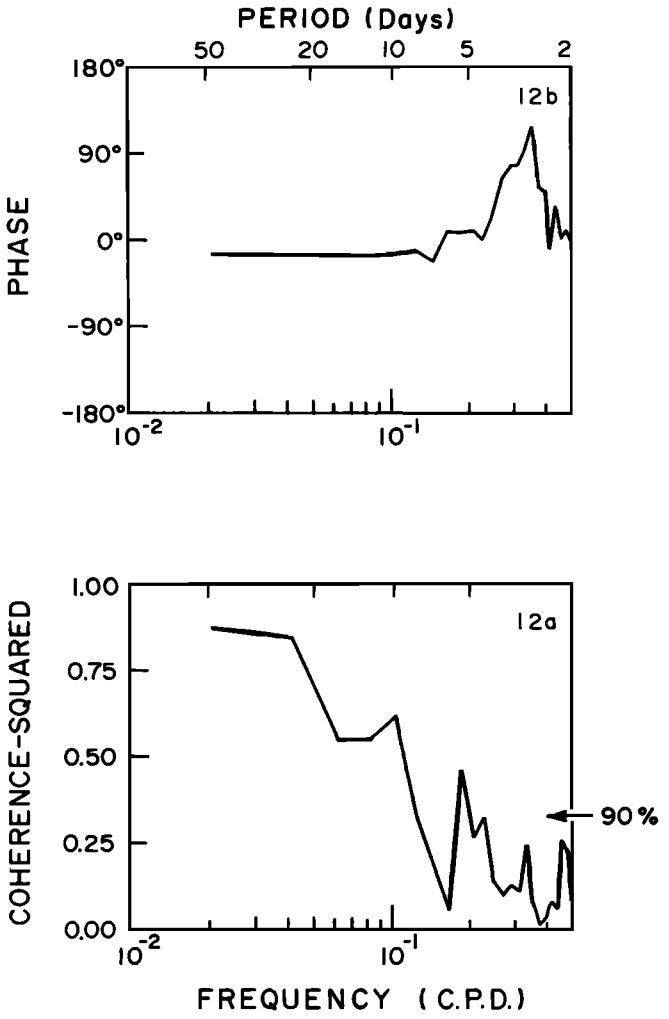

Fig. 12. (*a*) Coherence squared (γ^2) and (*b*) phase (ϕ) cross spectra of along-slope velocity component (u_b) between current meter sites 2 and 2L (1000 and 500 m off the bottom, respectively). The 90% confidence level for nonzero coherence squared is indicated by the arrow at the right of Figure 12*a*.

0.005, so the trajectory slopes are approximately 0.01 to 0.015. This slope is consistent with the kinematic bottom boundary condition $w = v_H \cdot \nabla_H h_b$ for average bottom slopes in this region $\partial h_b/\partial y_s \geq 0.01$. Estimates of the rms vertical velocity, using (7), are 2–3 × 10^{-2} cm/s, virtually identical to a purely kinematical estimate based on the product of the rms cross-slope velocity of approximately 2 cm/s and 10^{-2} bottom slope. This suggests vertical stretching is small within the lower 1000 m and, furthermore, implies a horizontal divergence of $0(10^{-7}\ s^{-1})$ within the upper 2000 m. Vertical velocities of $0(10^{-2})$ are consistent with Lagrangian estimates based on SOFAR float trajectories at shallower levels in the Gulf Stream (P. T. Shaw, personal communication, 1984).

The major results of this section are summarized in Figure 11. Leading segments of meander crests, as at AA', are associated with downslope flows and horizontal convergence; trailing segments, as at BB', are associated with upslope flows and horizontal divergence. For example, along the leading edge of a meander crest (AA'), advection of the deep isotherms by a velocity vector that is steeper than the isotherm slope results in an onshore displacement of the front; this is actually a result of downward and offshore advection of the isotherms. The reverse is true along the crest's trailing edge (BB'). As has been pointed out by *Chew* [1979] and *Lee and Atkinson* [1983], these cyclical patterns of upwelling and downwelling are consistent with a vorticity balance principally between vertical stretching and downstream changes in curvature vorticity. Domes of cold, upwelled water have been observed frequently between meander crests along the inshore edge of the Gulf Stream off the southeastern coast of the United States [cf. *Bane et al.*, 1981].

5. Topographic Rossby Waves

At each of the current meter sites there is a relative minimum in coherence between (Y, T) near 14 days (Figure 8). This is known to be an energetic period for topographic Rossby waves (TRW's) in this region [*Thompson*, 1977], and their presence may explain the lack of coherence between Gulf Stream displacements and deep temperature variability at these frequencies. In this section we examine briefly the characteristics of the low-frequency motions and show that they are consistent with TRW properties.

From the "Rise Array" data, *Thompson* [1977] has obtained good agreement between observed phase propagation of mo-

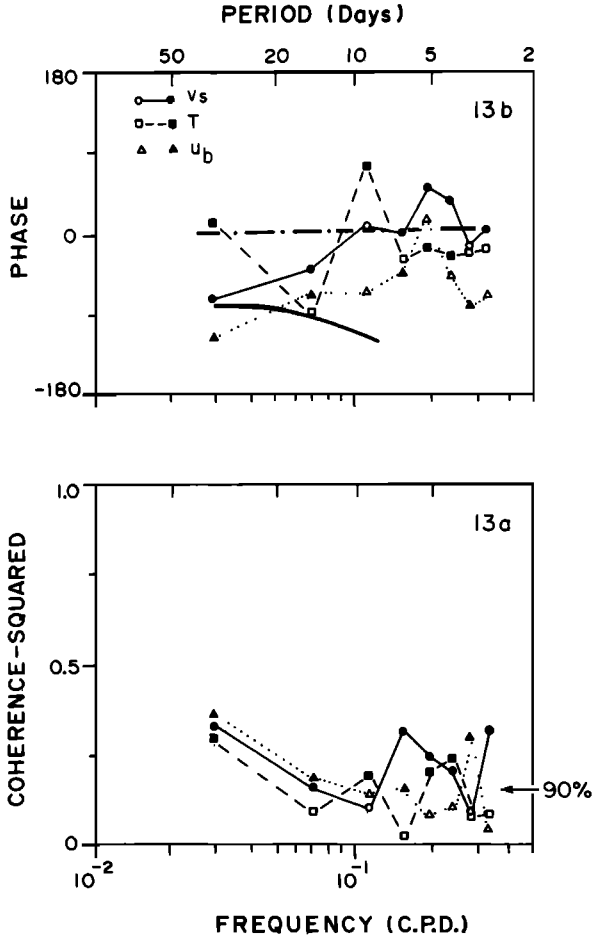

Fig. 13. (*a*) Coherence squared (γ^2) and (*b*) relative phase (ϕ) cross spectra of along-slope velocity component (u_b, triangles), cross-stream velocity (v_s, circles), and temperature (T, squares) between 9-month records at current meter sites 2 and 3. The closed symbols indicate points significantly coherent at the 90% confidence level. In (*b*) the bold solid line is the expected phase relationship for topographic Rossby wave propagation; the dash-dot line, for meander propagation, as in Figure 9. The 90% confidence level for nonzero coherence squared is shown at the right of (*a*).

TABLE 3. Eddy Statistics and Mean-Eddy Energy Conversions at Current Meter Sites

Site	Period Band, days	$\overline{u'^2}$, $cm^2\ s^{-2}$	$\overline{v'^2}$, $cm^2\ s^{-2}$	$\overline{T'^2}$, $°C^2 \times 10^{-4}$	$\overline{u'v'}$, $cm^2\ s^{-2}$	$\overline{v'T'}$, $°C\ cm\ s^{-1} \times 10^{-2}$	$-\overline{u'v'} \cdot \bar{u}_y$, $cm^2\ s^{-3} \times 10^{-6}$	$-g\alpha/\bar{\theta}_z \cdot \overline{v'T'} \cdot \bar{T}_y$, $cm^2\ s^{-3} \times 10^{-6}$
1	12–48	19.17	19.60	20.10	11.36 (0.59, 1.29)	0.56 (−8.48, 10.30)	7.95	4.28
	4–10	2.26	5.90	2.29	0.67 (−0.22, 2.17)	0.83 (0.04, 1.87)	0.47	6.21
2	12–48	20.44	9.62	22.20	5.98 (0.51, 1.40)	−1.49 (−1.40, 3.30)	4.20	−11.10
	4–10	1.19	1.71	1.34	0.17 (−0.42, 2.33)	−0.21 (−0.21, 2.14)	0.12	−1.61
2L	12–48	15.36	2.52	14.15	−0.29 (−4.40, 6.20)	−2.01 (0.24, 1.65)	−0.20	−15.10
	4–10	1.39	0.62	1.40	−0.43 (0.63, 1.30)	0.02 (−8.50, 10.50)	−0.30	0.13
3	12–48	19.38	13.14	21.58	10.51 (0.73, 1.20)	6.78 (0.38, 1.50)	7.35	50.82
	4–10	1.30	2.46	2.34	0.24 (−0.46, 2.38)	0.12 (−2.80, 4.80)	0.17	0.91

The numbers enclosed in brackets after each covariance estimate are factors by which the estimate is multiplied to obtain the 10% and 90% confidence limits of that covariance estimate.

tions with periods of 8–32 days and those predicted by *Rhines*' [1970] linear bottom-trapped topographic wave model. It can be shown [*Thompson and Luyten*, 1976] that for sufficiently short waves ($\lambda \leq 150$ km) the frequency of the bottom-trapped mode is given approximately by $\omega = \Gamma N \cdot \sin \psi$, where Γ is the bottom slope, N is the Brunt-Vaisala frequency, and ψ is the angle between the wave number vector and upslope. As frequency increases the phase propagates in a direction increasingly to the right of an observer facing downslope. The fluid velocity is in the plane of the wave fronts, so that in the zero-frequency limit the velocity fluctuations should be along the isobaths, and in the high-frequency limit the fluctuations should be up- and downslope. Observationally, the principal axes of variance and wave number vectors are very nearly perpendicular [*Thompson*, 1977]. For typical regional values of Γ (10^{-2}) and N (10^{-3} s) the shortest period to be expected is $2\pi/\Gamma N \sim 8$ days.

With only pairs of current meter sites occupied simultaneously, we are unable to compute wave number vectors. However, for periods greater than 12 days the principal axes are found to lie almost directly along the isobaths (Figure 5), suggesting a wave number vector pointing offshore. At all sites the low-frequency kinetic energy is distributed approximately equally between anticlockwise and clockwise rotating components. This suggests the oscillations are transverse, consistent with TRW kinematics.

The low-frequency currents at 500 and 1000 m off the bottom on mooring 2 are in phase and highly coherent. The coherence squared between the along-slope components u_b at these sites is shown in Figure 12. The coherence is significant for periods greater than 10 days, dropping off rapidly at periods shorter than the theoretical high-frequency cutoff near 8 days. *Hogg* [1981] has shown that the vertical distribution of kinetic energy near 70°W is more uniform beneath the axis of the Gulf Stream than on either the northern or southern sides. Interestingly, his results show a general increase in low-frequency kinetic energy with depth in the lower 1000 m, in contrast to the results at mooring 2. However, as noted in section 3, the three major events occurring in the record 500 m off the bottom on mooring 2 were in fact more energetic there than at 1000 m off the bottom.

The momentum flux (per unit mass) in the 10–48 day band is offshore, $\overline{u_b v_b} < 0$, at all sites, with magnitude $\sim 1\ cm^2/s^2$. An offshore momentum flux implies an energy flux toward shallower levels on the continental rise [*Rhines*, 1970], supportive of previous arguments by *Thompson* [1977] and *Hogg* [1981] that the Gulf Stream may act as an energy source for these fluctuations.

The phase propagation of TRW's should be offshore. Figure 9 plots the cross spectra of u_b and T between sites 1 and 2 and Figure 13 between sites 3 and 2. In each plot the leading series is the most western, upslope site, so negative phase implies eastward, offshore propagation. The relative phase of the velocity component u_b, essentially the principal axis component, should be a reliable indicator of TRW propagation [*Thompson*, 1977]. Sketched in the phase plots of Figures 9 and 13 are the "expected" phase relationships based on observed TRW dispersion parameters [*Thompson*, 1977; *Thompson and Luyten*, 1976]. The 3½-month cross spectrum between sites 1 and 2 is not really long enough to determine the propagation of low-frequency motions but has been included for completeness.

Between sites 1 and 2, both u_b and T show phase lags consistent with TRW propagation at the two lowest estimates, near 32 and 14 days. This may be fortuitous, since the u_b coherence is marginal at these frequencies. Between sites 3 and 2, the coherence of both u_b and T is significant near the 32-day period, dropping off to insignificant or marginal levels at higher frequencies. The propagation is offshore in the two lowest bands, with the exception of a near-zero phase estimate for temperature in the 32-day band, suggestive of along-stream meander propagation.

Overall, the measurements support offshore propagation. Beyond this the reliability of phase estimates is insufficient to establish any firm agreement or disagreement with details of TRW dispersion. The behavior of these low-frequency motions in the presence of the mean baroclinicity of the Gulf Stream as well as their possible interaction with Gulf Stream meanders are interesting problems for further study.

6. ENERGETICS

In this section we examine the classical barotropic and baroclinic energy exchange rates between the mean field and linear large-scale waves [*Brooks and Niiler*, 1977; *Webster*, 1961] to test whether these instabilities operate in the deep layers of the Gulf Stream. The barotropic and baroclinic conversion rates are $\overline{u'v'}\partial\bar{u}/\partial y$ and $g\alpha/|\overline{\theta_z}| \cdot \overline{v'T'}\partial\bar{T}/\partial y$, respectively [*Bryden*, 1979], where a negative value indicates transfer from the mean to the fluctuations. Of course a complete analysis of the energy transfers requires consideration of the full energy equation, as is treated nicely in *Brooks and Niiler* [1977] for the Florida Straits. In this section the covariances and conversion rates are computed in stream coordinates, with subscript s understood.

Table 3 lists estimates of these exchange rates within two frequency bands, with periods from 4 to 10 days and 12 to 48

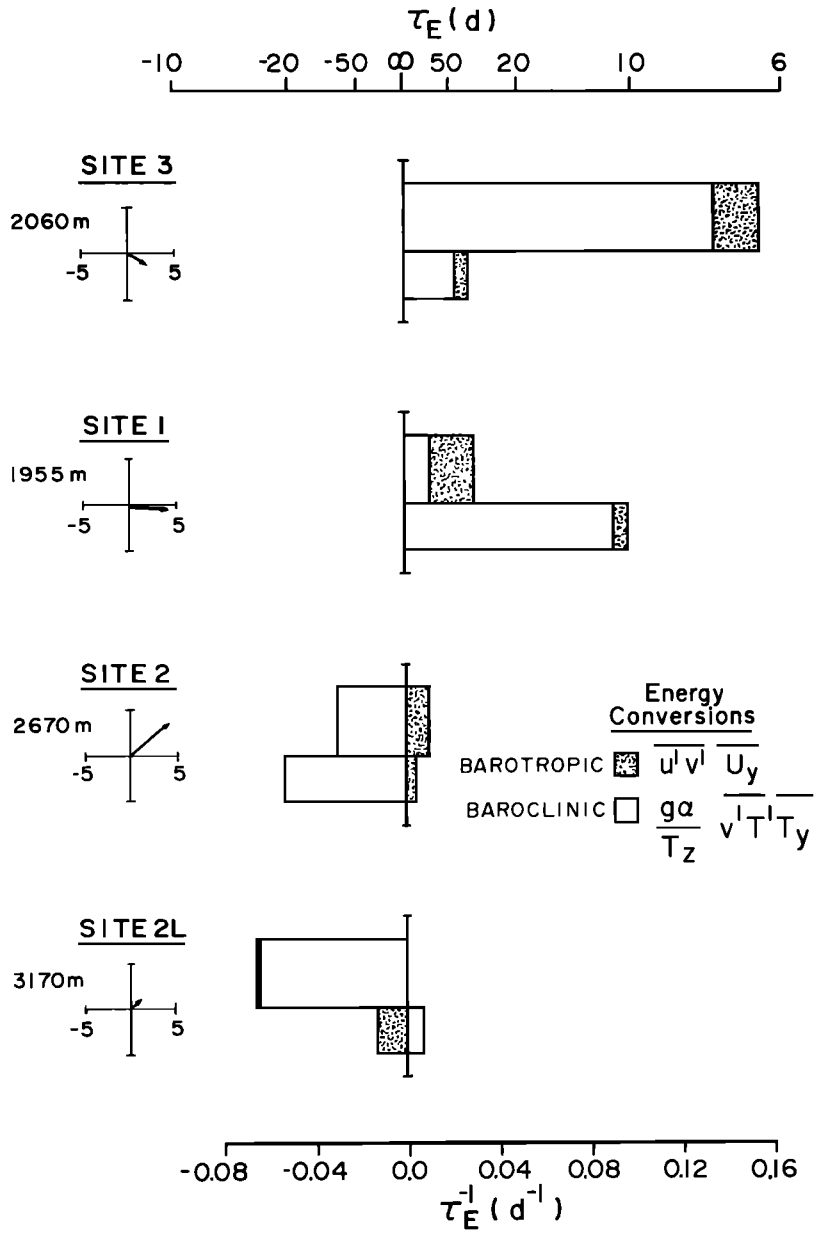

Fig. 14. Bar graph of energy *e*-folding time scales (τ_E) of mean-to-eddy energy conversion resulting from barotropic and baroclinic exchanges. At each site the upper bars indicate conversions within the 12–48 day band, and the lower bars indicate conversions within the 4–10 day band. The mean current (in cm/s) at each site is shown on left; the depth of the meter at each site is given on the far left.

days. Uncertainties in $\overline{u'v'}$ and $\overline{v'T'}$ are typically 40–120%, depending on the correlation coefficient and the length of the record. Most of the $\overline{u'v'}$ estimates in the 12–48 day band are significant, whereas there is greater uncertainty in the sign of the $\overline{v'T'}$ estimates (see Table 3). The mean cross-stream velocity gradient used in the calculation was $\partial\bar{u}/\partial y = -7 \times 10^{-7}$ s^{-1}, based on the means at sites 2 and 3; as before, $\partial\bar{T}/\partial y$ is taken to be 0.50×10^{-7}°C/cm.

The $\overline{u'v'}$ correlations are generally positive within both frequency bands. (The exception is the record 500 m off the bottom (site 2L), for which $\overline{u'v'} < 0$ in both bands.) Since $\partial\bar{u}/\partial y < 0$, the fluctuations here are gaining energy from the mean kinetic energy field. In almost all cases, however, energy conversion is dominated by the baroclinic term. The $\overline{v'T'}$ correlations are positive at sites 1 and 3 and generally negative at sites 2 and 2L. (The exception is the record 500 m off the bottom (site 2L), for which $\overline{vT'} > 0$ in the 4–10 day band.) Thus potential energy is transferred from the mean to the fluctuations at sites 1 and 3 and from the fluctuations to the mean at sites 2 and 2L.

Because our measurements are in deep water, the covariances in Table 3 are typically only 2% of those reported in shallower water off Onslow Bay [*Webster*, 1961; *Brooks and Bane*, 1981] or in the Florida Straits [*Brooks and Niiler*, 1977]. Thus the energy transfer rates in these deep waters are lower yet because the mean field gradients are also low. Figure 14 shows the energy *e*-folding time scale (τ_E) for the two frequency bands, obtained by dividing the barotropic and baroclinic conversion rates at each site by the eddy energy at that site. The sites are arranged in a way that emphasizes their geographic location relative to the cross-stream coordinate: site 3 is farthest shoreward, and sites 1 and 2 are successively

closer to the deep stream center but still on the cyclonic side. In the 12–48 day band the baroclinic conversion at site 3 is large and positive ($\tau_E \sim 8$ days); at site 1 it is much smaller, almost neutral ($\tau_E \sim 90$ days); and at sites 2 and 2L it is negative ($\tau_E \sim -33$ and -15 days, respectively). In the 4–10 day band there is a similar tendency, although the baroclinic conversion rate is largest at site 1 ($\tau_E \sim 11$ days). The barotropic conversion time scales are everywhere greater than 50 days.

These results suggest that baroclinic conversions of either sign dominate over barotropic conversions in deep water. One may compute the maximum deep-water transfers possible by either process, assuming that eddy potential energy is about equal to eddy kinetic energy (an observed fact) and that u',v' and v',T' are perfectly covariant. The associated e-folding time scales are then $(\frac{1}{2}\partial\bar{u}/\partial y)^{-1} \sim 33$ days for the barotropic term and $\{[(g\alpha/2\bar{\theta}_z)^{-1/2}]\cdot(\partial\bar{T}/\partial y)\}^{-1} \sim 3$ days for the baroclinic term, indicating that there is about 10 times more mean-state energy available to baroclinic than to barotropic conversion processes. Of course the actual covariances $\overline{u'v'}$ and $\overline{v'T'}$ are what is important, and as noted before, v and T are nearly in quadrature, making the baroclinic conversion rates much smaller than potentially possible. (The $\overline{v'T'}$ correlation coefficient is typically only 0.1 to 0.3.)

The spatial inhomogeneity across the stream of the baroclinic transfer makes it difficult to determine the direction of net energy transfer by this term. This is reminiscent of *Brooks and Niiler*'s [1977] results in the Florida Current showing baroclinic energy exchanges that were large locally but insignificant when averaged over the cross section. Upstream of our array, off Onslow Bay, measurements taken on the cyclonic side of the Gulf Stream indicate a transfer of energy from the fluctuations to the mean by both barotropic and baroclinic processes near the surface [*Webster*, 1961; *Oort*, 1964] and below the thermocline [*Brooks and Bane*, 1981]. This is a region characterized by meander amplitudes that decay in the direction of propagation [*Hood and Bane*, 1983]. There is little doubt, however, that in our study region meanders are growing rapidly, with temporal e-folding times ranging from 6 to 14 days (WJ82). Also, there is evidence near 70°W that low-frequency topographic Rossby waves may be growing, perhaps destabilized by the topography as theorized by *Pedlosky* [1980; *Hogg*, 1981]. Work by *Orlanski* [1969] and, more recently, by *Luther and Bane* [1985] has indicated that the dominant instability in the Gulf Stream should be of baroclinic type. In the latter work, significant energy conversion occurs primarily in thermocline layers where available mean potential energy is large [see also, *Hogg*, 1976]. Observations up in the thermocline are therefore necessary to determine whether the deep results reported here are, in fact, signatures of instability processes occurring farther up in the water column.

7. CONCLUSIONS

Our observations indicate that displacements of the Gulf Stream path are barotropic and in phase vertically between the surface and the deep flow. Deep temperature fluctuations are highly correlated with near-surface path displacements on the inshore edge of the Gulf Stream under the most steeply sloping part of the thermocline but less well correlated 50 km farther offshore within the body of the stream. The low coherence observed between deep temperature and velocity fluctuations over this 50 km cross-stream separation suggests a relatively short cross-stream scale here, an important consideration for future experiments in this region.

From these observations it has been possible to develop a consistent kinematical description of the relationship between Gulf Stream meanders and the deep velocity field in this region. Offshore movements of the stream's axis associated with the passage of meanders coincide with deep flows up the continental rise and vice versa. Kinematically, this requires cyclical vertical velocities of $0(10^{-2}$ cm/s), consistent with our estimates of vertical advection of temperature required to balance local rate of change of temperature and horizontal advection of temperature.

For periods longer than about 10 days the velocity spectrum in deep water is dominated by topographically controlled motions consistent with the properties of topographic Rossby waves. The energy associated with these motions is so large as to effectively mask deep velocity fluctuations that may be coherent with low-frequency displacements of the Gulf Stream path. This is a difficulty that will be resolved only by measurements up within the main thermocline where the mean velocity and temperature gradients are much larger.

Deep energy conversions between the mean field and the fluctuations in this region are dominated in magnitude by the baroclinic conversion term, with local energy e-folding time scales of 0(10 days). Time scales for energy conversion by the classical barotropic transfer, $\overline{u'v'}\partial\bar{u}/\partial y$, are longer (>50 days). At periods longer than 10 days the barotropic conversion is consistently from the mean to the fluctuations. The sign of baroclinic conversion, on the other hand, is more spatially variable. Thus, while baroclinic instability may be active in the deep Gulf Stream, a more extensive measurement array is required to estimate the net energy transfer by this process.

Acknowledgments. This work has been supported by the National Science Foundation under grants OCE78-09655, OCE79-21029, and OCE82-01222. We would like to thank Karen Lorenson, Elizabeth Johns, and Jorge Vazquez of the University of Rhode Island for their help and acknowledge the able assistance of the captain and crew aboard R/V *Endeavor* on several cruises, who helped to ensure our success. The inverted echo sounders were carefully prepared by Michael Mulroney. Special thanks go to James Sammonds for his help in preparing the current meters and moorings. General Oceanics Corp. (Miami, Florida) generously loaned us a Niskin winged current meter for this study.

REFERENCES

Bane, J. M., Jr., D. A. Brooks, and K. R. Lorenson, Synoptic observations of the three-dimensional structure, propagation, and evolution of Gulf Stream meanders along the Carolina continental margin, *J. Geophys. Res.*, *86*, 6411–6425, 1981.

Barrett, J., and W. Schmitz, Transport float measurements and hydrographic station data from three sections across the Gulf Stream near 67°W, *Tech. Rep. 71-76*, Woods Hole Oceanogr. Inst., Woods Hole, Mass., 1971.

Bendat, J. S., and A. G. Piersol, *Random Data: Analysis and Measurement Procedures*, Interscience, New York, 1971.

Brooks, D. A., and J. M. Bane, Jr., Gulf Stream fluctuations and meanders over the Onslow Bay upper continental slope, *J. Phys. Oceanogr.*, *11*(2), 247–256, 1981.

Brooks, D. A., and J. M. Bane, Jr., Gulf Stream meanders off North Carolina during winter and summer 1979, *J. Geophys. Res.*, *88*(8), 4633–4650, 1983.

Brooks, I., and P. P. Niiler, Energetics of the Florida current, *J. Mar. Res.*, *35*, 163–191, 1977.

Bryden, H. L., Momentum, mass, heat, and vorticity balances from oceanic measurements of current and temperature, Ph.D. thesis, 130 pp., Dep. Earth Sci., Mass. Inst. Technol./Woods Hole Oceanogr. Inst., Mass., 1975.

Bryden, H. L., Poleward heat flux and conversion of available potential energy in Drake Passage, *J. Mar. Res.*, *37*(1), 1–22, 1979.

Chew, F., Horizontal divergence, acceleration and curvature change, A diagnostic equation with applications, *Tellus, 31*, 548–557, 1979.
Duing, W., Synoptic studies of transients in the Florida Current, *J. Mar. Res., 33*, 53–73, 1975.
Duing, W., C. N. K. Mooers, and T. N. Lee, Low-frequency variability in the Florida Current and relations to atmospheric forcing from 1972 to 1974, *J. Mar. Res., 35*, 129–161, 1977.
Eady, E. T., Long waves and cyclone waves, *Tellus, 1*, 33–52, 1949.
Fofonoff, N. P., Spectral characteristics of internal waves in the ocean, *Deep Sea Res., 16*(suppl.), 59–71, 1969.
Hogg, N. G., On spatially growing baroclinic waves in the ocean, *J. Fluid Mech., 78*, 217–235, 1976.
Hogg, N. G., Topographic waves along 70°W on the Continental Rise, *J. Mar. Res., 39*(4), 627–649, 1981.
Hood, C. A., and J. M. Bane, Jr., Subsurface energetics of the Gulf Stream cyclonic frontal zone off Onslow Bay, August 1977, *J. Geophys. Res., 88*(8), 4651–4662, 1983.
Johns, W. E., Dynamics and structure of Gulf Stream meanders northeast of Cape Hatteras, Ph.D. thesis, Univ. R. I., Kingston, 1984.
Lee, T. N., Florida current spin-off eddies, *Deep Sea Res., 22*, 753–765, 1975.
Lee, T. N., and L. P. Atkinson, Low-frequency current and temperature variability from Gulf Stream frontal eddies and atmospheric forcing along the southeast U.S. outer continental shelf, *J. Geophys. Res., 88*(8), 4541–4568, 1983.
Luther, M. E., and J. M. Bane, Jr., Mixed instabilities in the Gulf Stream over the Continental Slope, *J. Phys. Oceanogr., 15*(1), 1985.
Luyten, J. R., Scales of motion in the deep Gulf Stream and across the Continental Rise, *J. Mar. Res., 35*, 49–74, 1977.
Oort, A. H., Computations of eddy heat and density transports across the Gulf Stream, *Tellus, 16*, 55–63, 1964.
Orlanski, I., The influence of bottom topography on the stability of jets in a baroclinic fluid, *J. Atmos. Sci., 26*(6), 1216–1232, 1969.
Pedlosky, J., The destabilization of shear flow by topography, *J. Phys. Oceanogr., 10*, 1877–1880, 1980.
Rhines, P. B., Edge, bottom, and Rossby waves in a rotating stratified fluid, *Geophys. Fluid Dyn., 1*, 273–302, 1970.
Richardson, P. L., and J. A. Knauss, Gulf Stream and western boundary undercurrent observations at Cape Hatteras, *Deep Sea Res., 18*, 1089–1109, 1971.
Robinson, A. R., J. R. Luyten, and F. C. Fuglister, Transient Gulf Stream meandering, 1, An observational experiment, *J. Phys. Oceanogr., 4*, 237–255, 1974.
Schmitz, W. J., Jr., A. R. Robinson, and F. C. Fuglister, Bottom velocity observations directly under the Gulf Stream, *Science, 170*, 1192–1194, 1970.
Thompson, R. O. R. Y., Observations of Rossby waves near Site D, *Progr. Oceanogr., 7*, 1–28, 1977.
Thompson, R. O. R. Y., and J. R. Luyten, Evidence for bottom-trapped topographic Rossby waves from single moorings, *Deep Sea Res., 23*, 629–635, 1976.
Warren, B. A., and G. H. Volkmann, Measurement of volume transport of the Gulf Stream south of New England, *J. Mar. Res., 26*(2), 110–126, 1968.
Watts, D. R., and W. E. Johns, Gulf Stream meanders: Observations on propagation and growth, *J. Geophys. Res., 87*, 9467–9476, 1982.
Webster, F. A., The effect of meanders on the kinetic energy balance of the Gulf Stream, *Tellus, 13*, 391–401, 1961.
Wright, W. R., and L. V. Worthington, The water masses of the North Atlantic Ocean; A volumetric census of temperature and salinity, *Serial Atlas of the Marine Environment*, folio 19, 8 pp., 7 plates, Am. Geogr. Soc., New York, 1970.

W. E. Johns and D. R. Watts, Graduate School of Oceanography, University of Rhode Island, Kingston, RI 02881.

(Received July 12, 1984;
accepted September 15, 1984.)